Electronic Supplementary Material (ESI) for Dalton Transactions.

The surface structure, stability, and catalytic performances toward O_2 reduction of CoP and $FeCoP_2$

Mengru Huang, Chunyan Sun, Xiangrui Zhang, Peijie Wang, Shusheng Xu, Xue-Rong Shi*

School of Material Engineering, Shanghai University of Engineering Science, 333 Longteng Road, Songjiang District, Shanghai, P. R. China

* Correspondence: shixuer05@mails.ucas.ac.cn

Method and models.

$O_2 + H^+ + e^- \rightarrow HOO^*$ (S1)

$HOO^* + H^+ + e^- \rightarrow O^* + H_2O$ (S2)

$O^* + H^+ + e^- \rightarrow HO^*$ (S3)

$HO^* + H^+ + e^- \rightarrow * + H_2O$ (S4).

For the associative reaction mechanism of ORR at pH = 0 and U = 0 V, the ΔG for each elementary step are calculated as follows.

$\Delta G_2 = G(O^*) + G(H_2O) - G(HOO^*) - 0.5G(H_2)$,

$\Delta G_3 = G(HO^*) - G(O^*) - 0.5G(H_2)$,

$\Delta G_4 = G(slab) + G(H_2O) - G(HO^*) - 0.5G(H_2)$, and given the fact that the high-spin ground state of the oxygen molecule is poorly described in DFT calculations, $\Delta G_1 = 4\times1.23 - (\Delta G_2 + \Delta G_3 + \Delta G_4)$. The free energy for water with gas phase was calculated at 0.035 bars because this is the equilibrium pressure in contact with liquid water at 298 K. The free energy of gas phase water at these conditions is equal to the free energy of liquid water. For the condensed phases, G(O*), G(HO*), G(HOO*), and G(slab), the temperature and pressure dependent items are small and tend to be neglected in the free energy calculation, then $G = E_{total} + ZPVE$. For the gaseous species, H_2 and H_2O molecule, besides the ZVPE, the enthalpies and entropies contributed by the transition, rotation and vibration, which was obtained from the Dmol3 code, are added too; $G = E_{total} + ZPVE + H - TS + RTln(P/P^0)$. E_{total} is the calculated electronic energies from the DFT. The calculated values of H and TS items are provided in Table S1. Note that the calculated H values obtained from the Dmol3 code in this work are the same as those calculated by $\int c_p dT$ method is Ref. [1].

Table S1. Free energies correction values (in eV) for gasphase H_2 and H_2O molecules at 298.15 K.

	ZPVE	H	-TS
H_2	0.27	0.09	-0.41
H_2O	0.58	0.10	-0.60

This work did not consider the electric field, and under this setting, there was no difference in the free energy of the ORR intermediates calculated in acidic and alkaline environment at fixed potential on the Reversible Hydrogen Electrode scale.[2]

Table S2. The optimized structure parameters of bulk $FeCoP_2$

$FeCoP_2$	d_{Fe-Fe} (Å)[a]	Lattice parameter (Å)
bulk-1	2.57, 2.57, 3.21	5.003, 3.203, 5.565
bulk-2	3.20, 3.20, 4.06	4.996, 3.204, 5.572
bulk-3	2.76, 2.76, 3.20	4.990, 3.203, 5.578

a: the shortest distance between two Fe atoms.

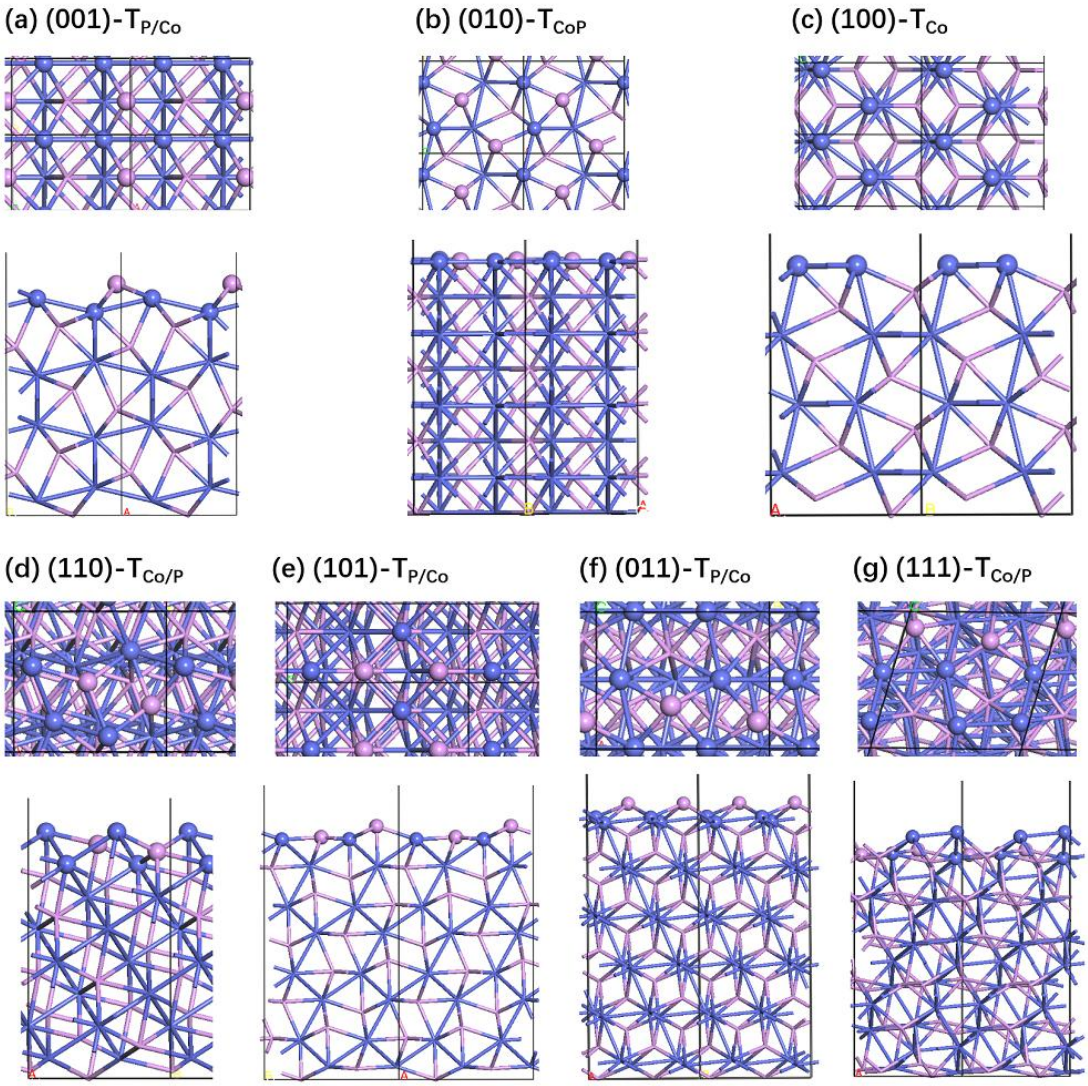

Figure S1. Full side (top) and top (bottom) views of optimized most stable termination structures of the low-index surfaces of CoP before optimization.

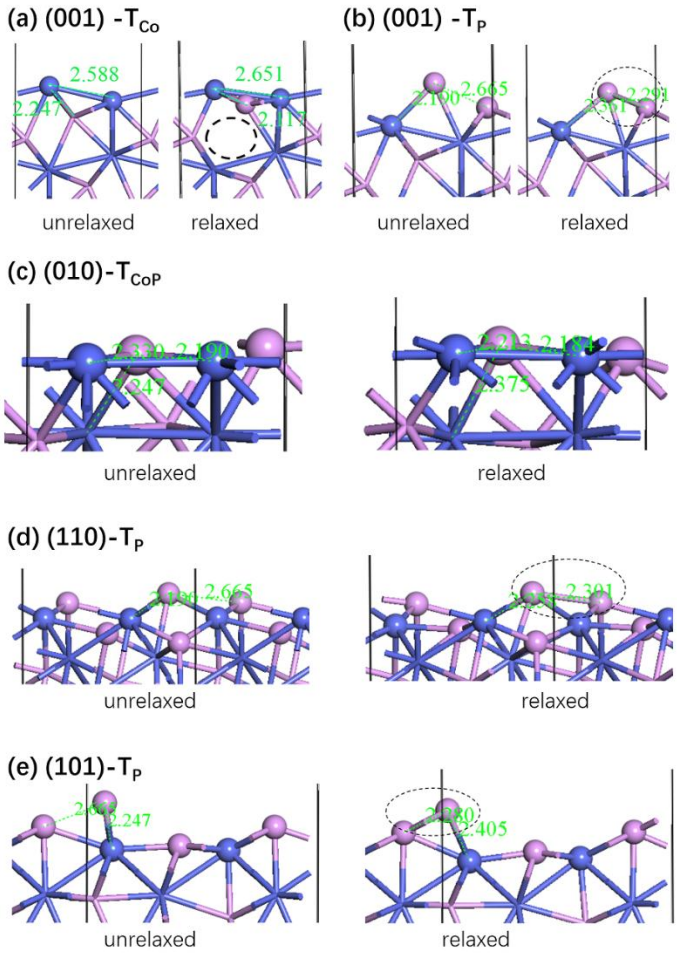

Figure S2. Comparison of surface structures of CoP before and after optimization. The key bond lengths are labelled (in Å). New formed bands or broken bond after optimization are marked in black dash circle.

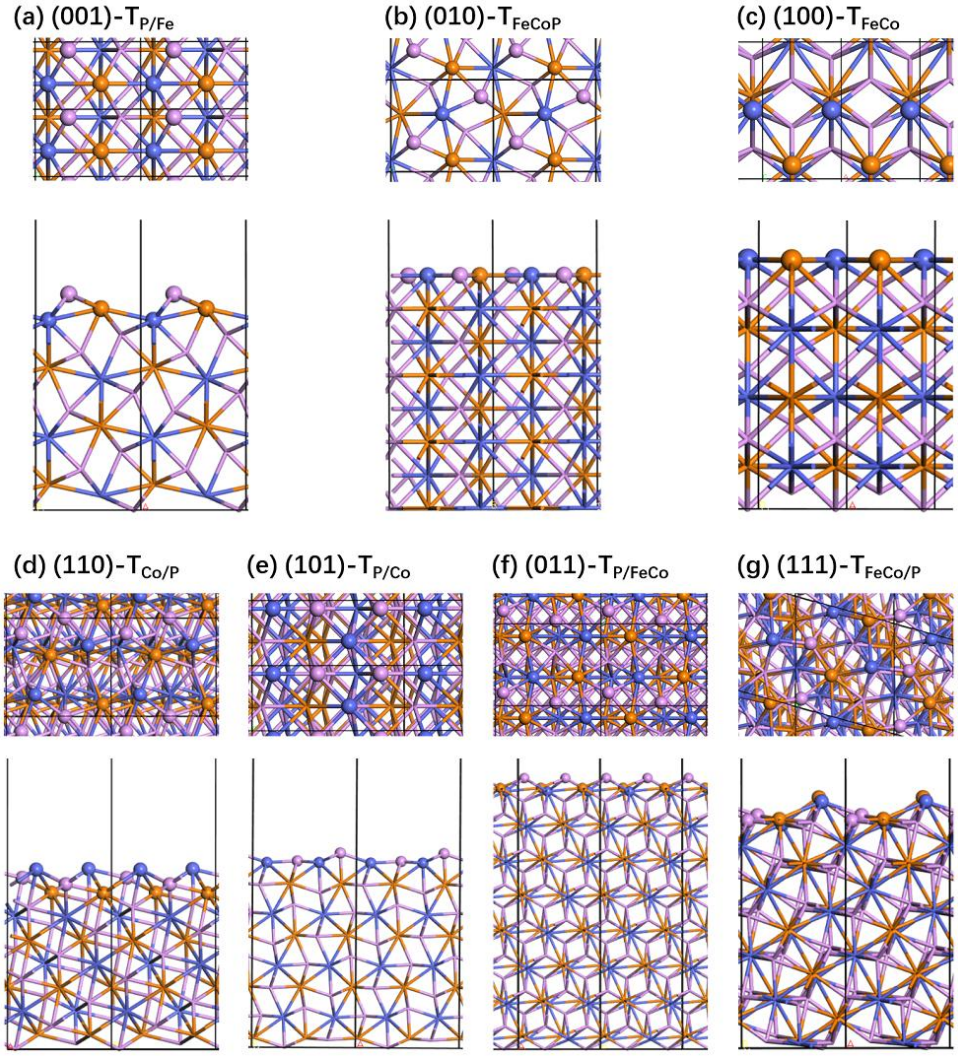

Figure S3. Full side (top) and top (bottom) views of optimized most stable termination structures of the low-index surfaces of $FeCoP_2$ before optimization.

Table S3. The magnetic moment of optimized structures.

	bulk	(101)	(011)	(111)	(001)
CoP	0	0	0	1	0
$FeCoP_2$	0	2	3	4	0

Adsorption site.

For the (101) surfaces, the adsorption sites including four top sites (t_{Co1}, t_{Co2}, t_{P1} and t_{P2}), seven bridge sites ($b_{Co1\text{-}Co1'}$, $b_{Co1\text{-}P1}$, $b_{Co1\text{-}P2}$, $b_{Co2\text{-}P1}$, $b_{Co2\text{-}P2}$, $b_{P1\text{-}P1'}$, and $b_{P2\text{-}P2'}$) and one hollow site: $h_{P1\text{-}Co2'\text{-}P2\text{-}Co2}$) have been considered. For HOO species, the most stable adsorption site is the top site of P1. For HO and H, the most stable adsorption site is the bridge site of Co1-P1.[3] For the (011) surface, five top sites (t_{Co1}, t_{Co2}, t_{Fe1}, t_{Fe2} and t_{P1}) and nine bridge site ($b_{Co1\text{-}P1}$, $b_{Co2\text{-}P1}$, $b_{Fe1\text{-}P1}$, $b_{Fe2\text{-}P1}$, $b_{Co1\text{-}Fe1}$, $b_{Fe1\text{-}Co2}$, $b_{Co2\text{-}Fe2}$, $b_{Co1\text{-}Fe2}$, $b_{Co2\text{-}Fe2'}$).

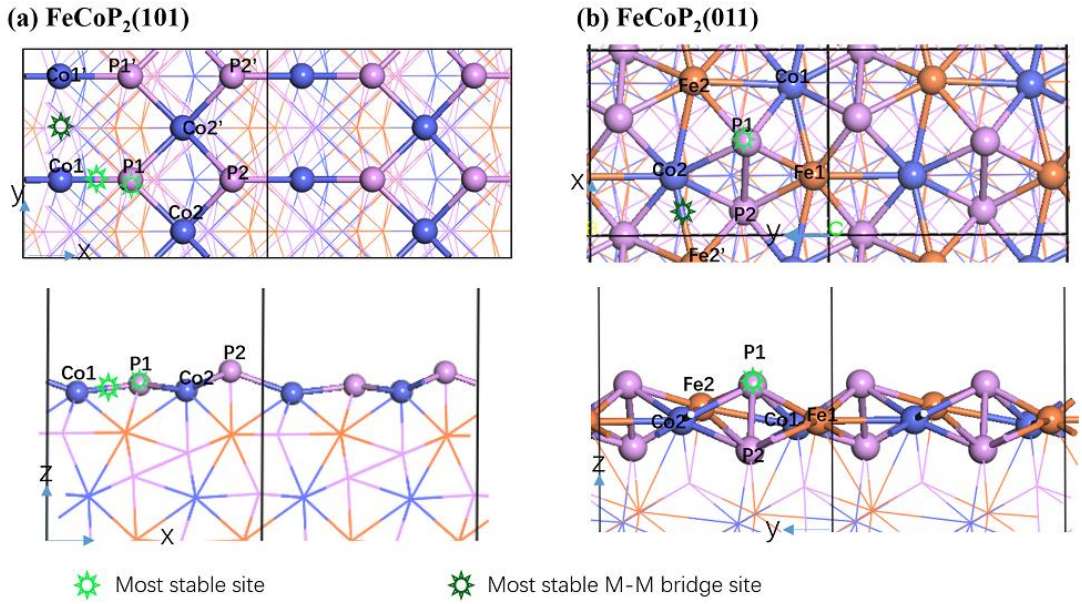

Figure S4. Adsorption site on $FeCoP_2$(101) and (011) surfaces.

Table S4. The total energy difference (eV) of species adsorption on the most and second most stable site with and without the solvent effect involved.[a]

	CoP(101)		$FeCoP_2$(101)		CoP(011)		$FeCoP_2$(011)	
	$b_{P\text{-}Co}$	$b_{Co\text{-}Co}$	$b_{P\text{-}Co}$	$b_{Co\text{-}Co}$	t_P	$b_{Co\text{-}Co}$	t_P	$b_{Fe\text{-}Co}$
OH	-0.17	-0.05	-0.16	-0.03	-0.17	-0.05	-0.17	-0.04
O	-0.001	-0.01	-0.02	-0.01	-0.12	-0.01	-0.12	-0.02
OOH	-0.16[b]	-0.08	-0.04[b]	-0.11	-0.17	-0.05	-0.17	-0.07

a: $E_{difference} = E_{total}(sol) - E_{total}(without\ sol)$. b: the most stable adsorption site shifted to the top site of surface P.

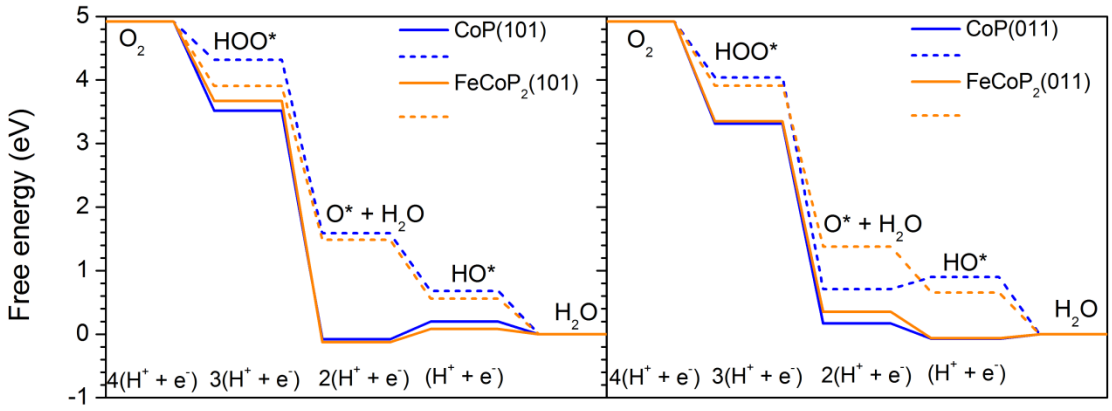

Figure S5. Free energy profiles of ORR on (101) and (011) surfaces excluding the contribution of the solvent effect. Solid lines: ORR occurs on the most stable site. Shot dash lines: and ORR occurs on the second most stable site.

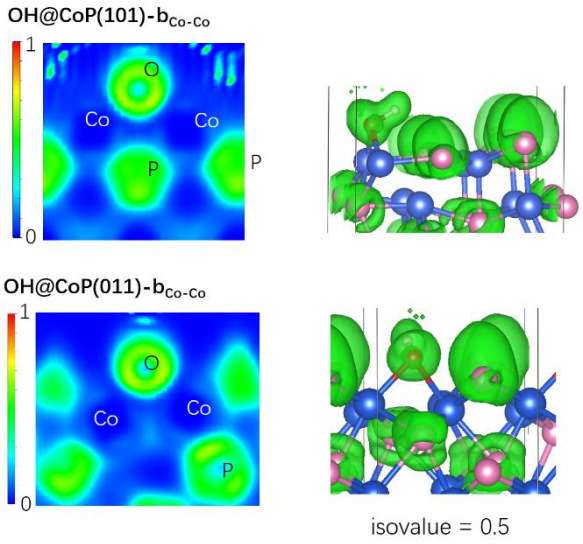

Figure S6. ELF of HO adsorption on the metal-metal bridge site of (101) and (011) surfaces of CoP. The cutting plane for 2D plot (left) is the best-fitting plane of three bonding metal-metal-O atoms. For 3D plot (right), the isovalue is 0.5.

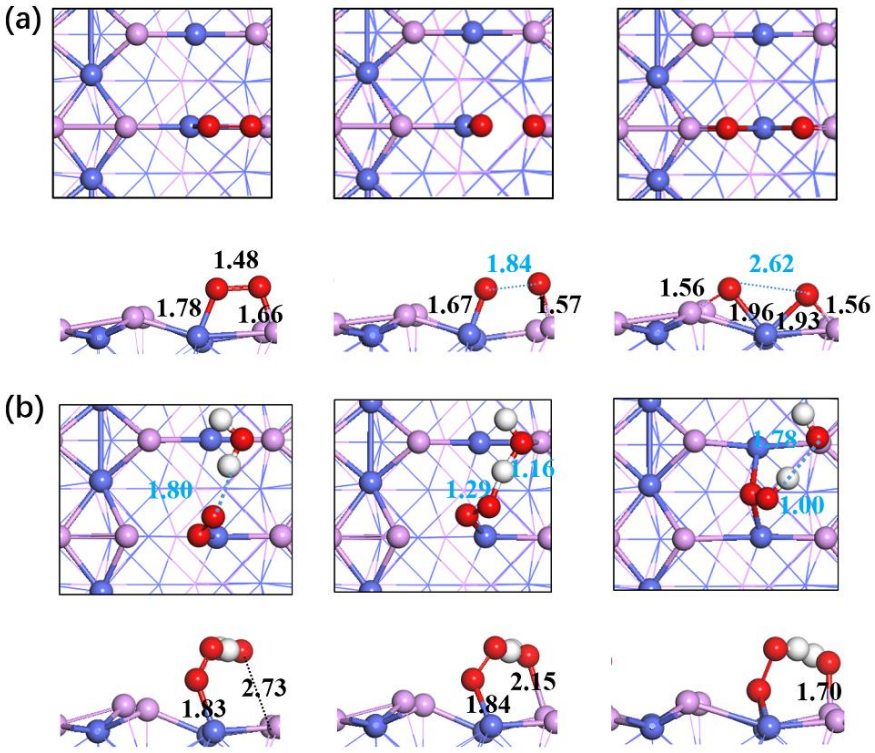

Figure S7. The top and side views of (a) O_2 direct dissociation and (b) O_2 hydrogenation reaction pathways. Left: reactant, middle: transition state, right: product. The key distances are labelled (in Å).

Reference

1 S. Back, M. H. Hansen, J. A. Garrido Torres, Z. Zhao, J. K. Nørskov, S. Siahrostami and M. Bajdich, *ACS Appl Mater Interfaces*, 2019, **11**, 2006–2013.

2 J. Rossmeisl, Z. W. Qu, H. Zhu, G. J. Kroes and J. K. Nørskov, *J Electroanal Chem*, 2007, **607**, 83–89.

3 Y. N. Wang, Z. J. Yang, D. H. Yang, L. Zhao, X. R. Shi, G. Yang and B. H. Han, *ACS Appl Mater Interfaces*, 2021, **13**, 8832–8843.